Journal of Power Sources 195 (2010) 6016–6023

Contents lists available at ScienceDirect

Journal of Power Sources

journal homepage: www.elsevier.com/locate/jpowsour

Catalytic gasification of automotive shredder residues with hydrogen generation

Kuen-Song Lin*, Sujan Chowdhury, Ze-Ping Wang

Department of Chemical Engineering and Materials Science/Fuel Cell Center, Yuan Ze University, Chung-Li City 320, Taiwan, ROC

ARTICLE INFO

Article history:
Received 10 January 2010
Received in revised form 8 March 2010
Accepted 27 March 2010
Available online 14 April 2010

Keywords:
Automotive shredder residues
Catalytic gasification
Reforming
Syngas
Hydrogen generation
Fuel cell

ABSTRACT

Hydrogen is a clean and new energy carrier to generate power through the Proton exchange membrane fuel cell (PEMFC) system. Hydrogen can be effectively turned out through the catalytic gasification of organic material such as automotive shredder residues (ASR). The main objective of this manuscript is to present an analysis of the catalytic gasification of ASR for the generation of high-purity hydrogen in a lab-scale fixed-bed downdraft gasifier using 15 wt.% NiO/Al_2O_3 catalysts at 760–900 K. In the catalytic gasification process, reduction of Ni(II) catalyst into Ni(0) has been confirmed through XANES spectra and consequently EXAFS data shows that the central Ni atoms have Ni–O and Ni–Ni bonds with bond distances of 2.03 ± 0.05 and 2.46 ± 0.05 Å, respectively. ASR is partially oxidized and ultimately converts into hydrogen rich syngas (CO and H_2) and increases of the reaction temperature are favored the generation of hydrogen with decomposition of the CO. As well, approximately 220 kg h^{-1} of ASR would be catalytically gasified at 760–900 K and 46.2 atm with the reactor volume 0.27 m^3 to obtain approximately 3.42×10^5 kcal h^{-1} of thermal energy during over 87% syngas generation with the generation of 100 kW electric powers.

1. Introduction

The heavier recyclable metals of automobiles have been substituted by lighter weight plastics, textiles or rubbers in recent years. The shift to increase plastic/rubber usage may soon make the metal shredding process less economical. Automotive shredder residues (ASR) are mostly consisting of plastics or rubbers and usually obtain from the automobile recycling process to facilitate the recovery of the metals. It has the problematic characteristics of a complex waste stream and that makes it difficult for treating processes [1–3]. Over 0.5 million tons per year (TPY) of ASR were produced in Taiwan in the last decade [1]. The results of typical compositions of ASR mixtures in Taiwan are shown in Table 1, in which light ASR components contain higher portion of the fine inorganic materials over 70 wt.% and heavy ASR components are observed around at 88 wt.%. Additionally, the main components in bulk materials of light and heavy ASRs are both plastics, textiles or rubbers containing over 20 and 80 wt.%, respectively [2–5]. ASR has been considered a recoverable waste; on the other case improper disposal of could cause negative environmental impact and disease problem. Like most other organic materials, an ASR encloses a high amount of organic volatiles and including hydrogen [2–5]. Thus, gasification of ASR has been known as one of effective technology options for the utilization of renewable hydrogen energy resources [6–8].

Hydrogen, a clean and new energy carrier for the future, is usually generated by chemical conversion of fuels such as hydrocarbons or organics [9,10]. In addition, the effective and active catalysts in the ASR gasification have the advantages of resisting carbon attrition and deactivation [11–13]. Catalytic gasification of ASR to produce synthesis gas and heat energy may be an appealing resource recovery alternative. The main challenges of implementing and improving catalytic gasification technology are to develop a suitable catalyst for enhancing synthesis gas (syngas, $CO + H_2$) yield to generate power with an integrated fuel processor such as a Proton Exchange Membrane Fuel Cell (PEMFC) system. In previous works, some catalytic systems have been investigated including metal oxides, active metals or cheap minerals for the ASR gasification process [14–23]. Comparatively, the best activity with short contact time, high conversion ratio or use of inexpensive nickel catalysts supported on zeolites, Al_2O_3 or CeO_2 were found [24–33]. Nickel catalyst is the well-known attractive catalyst among metals like Co, Fe, Pt, Ru or Rh due to the performance and economical reason [14,34,35]. However, nickel catalyst can be used effectively after reducing the catalyst deactivation and erosion problem. Stronger interaction between NiO and support can restrain the loss and deactivation such like sintering of nickel [35–37]. To develop more stable catalysts, alumina-based material can be act as a primary support for decreasing the catalyst deactivation. Nickel based catalysts are also deactivated due to the catalytic poisoning. Strong chemisorptions of impurities (mainly H_2S or SO_x) are occurred onto the catalyst active sites and then deactivate the catalyst [38]. Forzatti and Lietti [39] have reported

* Corresponding author. Tel.: +886 34638800x2574; fax: +886 34559373.
E-mail address: kslin@saturn.yzu.edu.tw (K.-S. Lin).

0378-7753/$ – see front matter © 2010 Elsevier B.V. All rights reserved.
doi:10.1016/j.jpowsour.2010.03.084

Table 1
Typical compositions of ASR mixtures in Taiwan.

	Light ASR[a]	Heavy ASR[b]
Fine materials (<10 mm) (wt.%)		
Small pieces (soil, glass, sand, ceramic, inorganics, etc.)	70.45	7.84
Bulk materials (wt.%)		
Hard plastics	8.20	29.41
Soft plastics	1.65	2.96
Formed polystyrene	1.12	0.28
Textile/fabrics/fibers	8.34	10.47
Rubber	3.52	32.47
Formed rubber	4.98	2.96
Tires	0.84	8.22
Wood/biowastes	0.57	4.74
Wire/steel/non-ferrous metals	0.33	0.65

[a] "Light ASR" denotes the lighter fraction separated from the total product shredded in the first step using simple suction (17–22 wt.% of the total product shredded).
[b] "Heavy ASR" denotes the component which is left after ferrous metals are magnetically removed from the non-sucked stream (8–11 wt.% of the total product shredded).

that sulfur adsorption decreases with increasing temperature and conditioning the feed gas to the catalyst can prevent poisoning and significantly increase gas formation. In addition a fuel processing is defined as conversion of any hydrocarbons or organics to a fuel gas and this reformation is suitable for a PEMFC anode reaction system [40–44]. In an integrated PEMFC, ASR can be processed to produce H_2-rich syngas through several steps including reforming, steam reforming or water gas shift reaction, and preferential oxidation. Furthermore, H_2/oxygen (or air) mixture is fed to the PEMFC stack for a direct electric current generation and then is converted to an alternating electric current by the power conditioner [43–45]. The role and effect of suitable catalyst such as nickel oxide alumina support on catalytic performance to generate syngas for the implication of power generation has not been clearly investigated. More importantly, development of more effective gasification methods based on highly active nickel catalysts has been paid great attention, due to the recover of hydrogen or CO in syngas [33–39]. Therefore, the main objective of the present work was to assess the feasibility of ASR catalytic gasification with syngas recycling for the potential application on an integrated fuel processor (e.g. PEMFC) system. The physicochemical properties, morphology, and fine structures of ASR, product gases and 10–15 wt.% NiO/Al_2O_3 catalysts were measured and identified. In addition, cost or benefit analysis of the ASR catalytic gasification was also performed to confirm the economic feasibility for such a recycling practice and determine if further development would be warranted.

2. Experimental

2.1. Catalyst preparation

Reagents were obtained as American Chemical Society (ACS) grade with purity > 99%. About 10 g support of well-milled high surface area Al_2O_3 ultrafine particles were mixed with 7–10 g $Ni(NO_3)_2{\cdot}6H_2O$ in 30 mL water solution for the preparation of the 10–15 wt.% NiO/Al_2O_3 (ASR/catalyst wt. ratio = 50 and molar steam-to-oxygen-to-carbon ratio (S/O/C) = 1.4/1.2/1.0) catalysts by impregnation method. Water was evaporated and the resulted solid residues were calcined under a flowing air for 5–8 h at 873 K. In addition, the Ni concentrations of as-synthesized catalysts were also identified and calculated using atomic adsorption spectroscopy (AAS, PerkinElmer AA200) and inductively coupled plasma-optical emission spectroscopy (ICP-OES, PerkinElmer Optima 2100DV).

2.2. Lab-scale ASR catalytic gasifier

In a lab-scale downdraft-type reactor (enclosed in electrically heated jackets) was operated under isothermal and isobaric conditions to obtain the catalytic reforming tests of ASR. ASR catalytic gasification system has been conducted (feed rate of 100 kg h^{-1}) at 760–900 K (average operating temperature of 830 K) with a mixing flow of 10.5–21.0 vol.% O_2 and steam (gas hourly space velocity (GHSV) = 50,000 h^{-1} at STP). All parts and connections used in the gasifier were brass or stainless steel, and the gas inlet and outlet flow systems were well sealed with polyethylene tubes. The catalytic gasifier was a stainless steel tube with 2.54 cm i.d. and 60 cm long and operated the gasifier at O/C atomic ratios between 1.10 and 1.30. A separation stainless steel filter (300 meshes) was added between catalyst and the glass wool to trap the ashes and therefore significantly lower amount of ashes was deposited onto the catalyst. In addition, the durability of all the NiO/Al_2O_3 catalysts for ASR gasification was over 24 h and the used catalysts were also further identified as field emission-scanning electron microscopy (FE-SEM) or transmission electron microscopy (TEM) techniques. Noncondensible gases generated in the catalytic gasifier were passed through a water cooler and measured by using a totalizer. The condensates were separated and collected in the two knockout drums (500 and 300 mL) in series. The noncondensible gases were sampled and analyzed by an *on-line* Digilab Fourier transform infrared spectroscopy (FTIR) spectrometer (FTS-40) and then scrubbed with 1 M NaOH solutions before emitting.

2.3. Thermogravimetric analyses and kinetics of ASR

Preliminary studies and basic engineering design of catalytic gasification of ASR with 15 wt.% NiO/Al_2O_3 catalyst (ASR/catalyst wt. ratio = 50 and molar steam-to-oxygen-to-carbon ratio (S/O/C) = 1.4/1.2/1.0) were investigated using a thermogravimetric analyzer (TGA) (model SDT 2960 & Thermal Analyst 2000, TA Instruments). Reaction temperatures and ASR/catalyst sample weights were recorded at 10 s intervals. About 50 mg of samples were heated from 400 to 973 K at a heating rate of 5, 10 or 15 K min^{-1} with a sensitivity of 0.1 ± 0.01 μg in a mixing flow of 10.5–21.0 vol.% O_2 and steam (100 mL min^{-1}) in the TGA. The calibration procedures were performed once a month, including TGA weight calibration, DTA (differential thermal analysis) baseline calibration, and temperature calibration. In all experiments, aluminum oxide was used as a reference. Gasification kinetic parameters derived from the TGA data (such as activation energy and pre-exponential factor) were based on the classical laws of kinetics. Detailed descriptions of the method have been given by Petrović and Zavargo [46] or Friedman [47] covered important techniques for evaluating the kinetic parameters from the TGA traces. The overall rate equation of conversion factor expressed in the Arrhenius relation form for an ASR catalytic gasification reaction is as

following:

$$\ln\left(\frac{dX}{dt}\right) = \ln A_p + n\,\ln(1-X) + \left(-\frac{E_a}{RT}\right) + m\,\ln[O_2]$$

$$X = \frac{W_0 - W}{W_0 - W_f}, \quad k = A_p\,\exp\left(-\frac{E_a}{RT}\right)$$

where t is the reaction time (min), A_p is the pre-exponential factor (min^{-1}), E_a is the activation energy (kcal mol^{-1}), k is the Arrhenius rate constant, T is the reaction temperature (K), R is universal gas constant (1.987×10^{-3} kcal g^{-1} mol^{-1} K^{-1}), W is the mass of ASR sample at time t, $g(O_2)$ is the mth order for the oxygen composition, $f(X)$ is the nth order for the unreacted ASR, and W_o and W_f are the initial and final (or residual) mass of ASR samples, respectively.

2.4. Characterization methods of ASR and catalysts

Proximate and ultimate analyses of ASR compositions were performed in the initial stage using traditional elemental analyzer (EA, F002-heraeus rapid CHN-O) shown in Table 2. The compositions of gas products for ASR catalytic gasification, such as syngas ($CO + H_2$), were analyzed by using GC (Agilent, 6890N) and FTIR spectroscopy (10-cm gas cell). Infrared spectra were recorded on a Digilab FTIR spectrometer (FTS-40) with fully computerized data storage and data handling capabilities. For all spectra reported, a 64-scan data accumulation was conducted at a resolution of 4 cm^{-1}.

Morphologies and microstructures of NiO/Al_2O_3 catalysts were determined by FE-SEM/EDS (Hitachi, S-4700 Type II). TEM analysis was conducted to investigate the crystallinity and particle size distribution of the catalyst samples with a model Zeiss 10C using 150 kV accelerating voltage. The BET surface area of NiO/Al_2O_3 catalysts for ASR gasification was obtained from the conventional analysis of N_2 isotherms measured at 77 K with ASAP2020 (Micromeritics Surface Area and Porosity Analyzer). All the catalyst samples were degassed at 100 °C prior to the measurement. The surface area of the as-synthesized 10–15 wt.% NiO/Al_2O_3 catalysts ranges from 125 to 150 m^2 g^{-1}.

Table 2
Proximate and ultimate analyses of typical ASR mixtures in Taiwan.

	Light ASR[a]	Heavy ASR[b]
Proximate analysis (wt.%)		
Volatile	60.83	57.64
Fixed carbon	9.66	19.92
Moisture	2.64	1.88
Ash	26.87	20.56
Ultimate analysis (wt.%)		
Carbon	64.22	71.74
Hydrogen	6.46	7.89
Nitrogen	1.94	2.78
Sulfur	0.72	0.98
Chlorine	1.23	2.16
Oxygen	Balanced	Balanced
True specific density (20/4 °C)	1.28	1.34
Bulk specific density (g cm^{-1})	0.15	0.54
High heating value (kcal kg^{-1})	5340	11,465

[a] "Light ASR" denotes the lighter fraction separated from the total product shredded in the first step using simple suction (17–22 wt.% of the total product shredded);.
[b] "Heavy ASR" denotes the component which is left after ferrous metals are magnetically removed from the non-sucked stream (8–11 wt.% of the total product shredded).

X-ray absorption near-edge structural (XANES)/extended X-ray absorption fine structural (EXAFS) spectra of nickel catalysts were collected at Wiggler 17C1 beamline of Taiwan National Synchrotron Radiation Research Center (NSRRC). The electron storage ring was operated with the energy of 1.5 GeV and a current of 100–200 mA. A Si(111) DCM was used for providing highly monochromatized photon beams with energies of 1–15 keV and resolving power of up to 7000. Data were collected in fluorescence or transmission mode with a Lytle ionization detector [48] for Ni (8333 eV) K-edge experiments at room temperature. The photon energy was calibrated by characteristic pre-edge peaks in the absorption spectra of Ni stan-

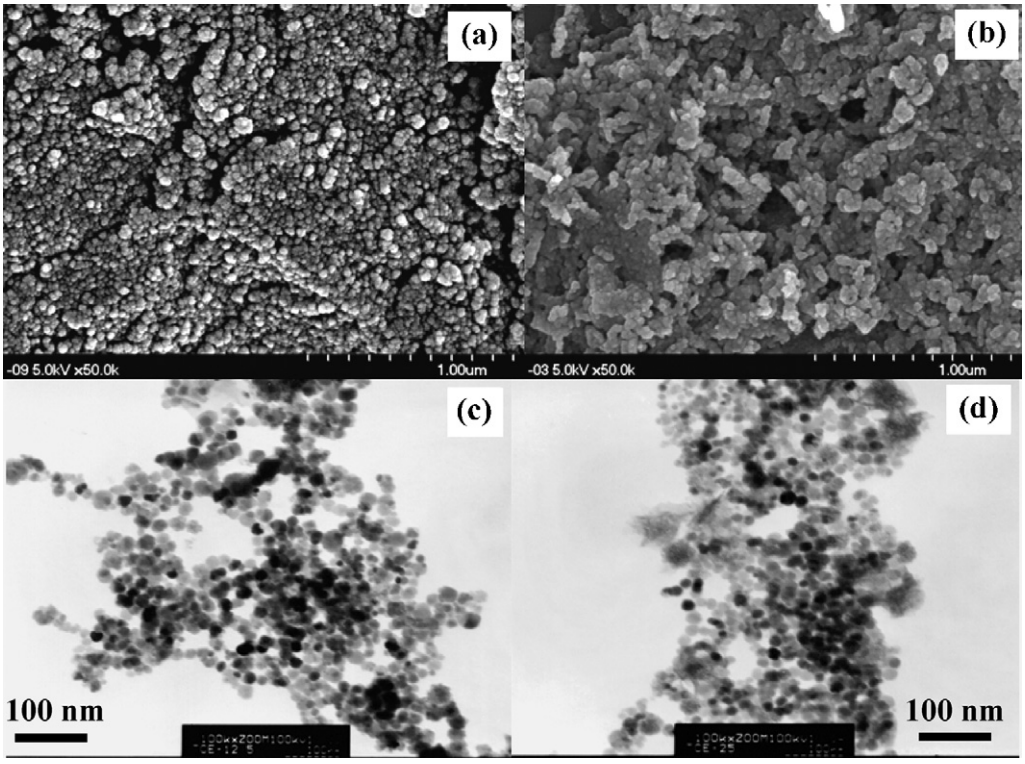

Fig. 1. FE-SEM and TEM microphotos of fresh (a and c) and used (b and d) of 15 wt.% NiO/Al_2O_3 catalyst, respectively for an ASR catalytic gasifier at T = 900 K and 1 atm.

dard. Raw absorption data in the region of 50–200 eV below the edge position were fit to a straight line using the least-square algorithms. The fitted pre-edge background curves were extrapolated throughout all data range, and subtracted and normalized to minimize the effect of catalyst sample thickness with respect to the edge jump by using program package AUTOBK. Near-edge structure in an absorption spectrum covers the range between the threshold and the point at which the Ni EXAFS begins. The Ni XANES extend to the energy of the order of 50 eV above the edge. The k^2-weighted and EXAFS spectra were Fourier transformed to R space over the range of 2.5–12.5 $Å^{-1}$. Ni EXAFS data were analyzed by UWXAFS 3.0 program and FEFF 8.0 codes [48–50].

3. Results and discussion

3.1. Catalyst characterization

Generally, nickel nanoparticles are used to take participation for hydrogen formation in the higher reaction temperature [27]. Notably visualized spherical or irregular shape NiO/Al_2O_3 nanocatalyst includes a diameter of approximately 10–20 nm is shown in Fig. 1(a) through FE-SEM microphotograph. As shown in Fig. 1(c), TEM image also indicates that fresh nickel nanoparticles are well dispersed in the microstructures of Al_2O_3 support and the particle size is confirmed. Furthermore, FE-SEM and TEM analysis reveal that the nickel nanoparticles are highly dispersed on the surface of Al_2O_3 supporter. The size of the NiO nanoparticles is a very important factor as to determine the activity of the catalyst. Significant amount of NiO have reduced to metallic Ni after gasification reaction as shown in Fig. 1(b) and (d), respectively. A few darker spots suggest that the reduced Ni concentrations occur in certain areas with the particle size around 25–35 nm. The above results suggest that the temperature has a significant effect for the crystal migration behavior to increase the size of the catalyst.

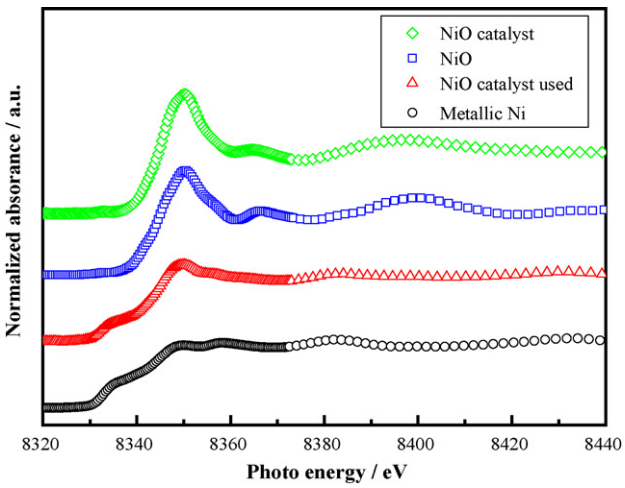

Fig. 2. XANES spectra of Ni/NiO standards and fresh/used nanophase 15 wt.% NiO/Al_2O_3 catalysts for an ASR catalytic gasifier at 900 K and 1 atm.

XANES and EXAFS spectra of Ni(0) or Ni(II) on Al_2O_3 in the ASR catalytic gasification process were studied (Figs. 2 and 3) for thoroughly examine the nature of the catalyst. The XANES spectroscopy

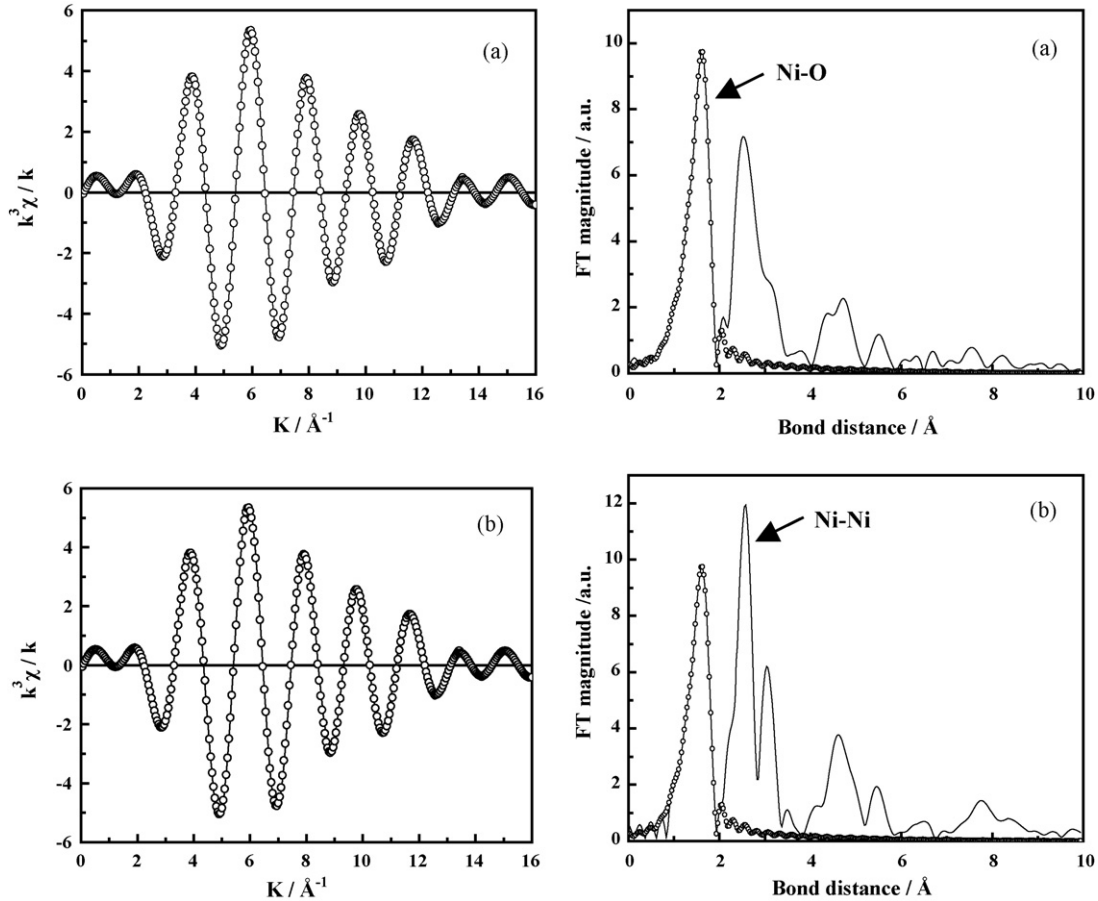

Fig. 3. Ni K-edge EXAFS oscillation $k^2\chi(k)$ and Fourier transform (FT) spectra of (a) fresh and (b) used 15 wt.% NiO/Al_2O_3 catalysts for an ASR catalytic gasifier at 900 K and 1 atm. The best fitting of the EXAFS spectra are expressed by the dotted lines.

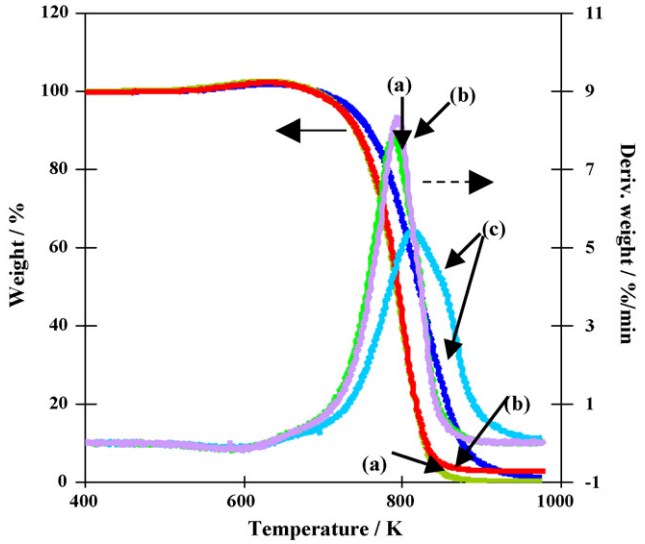

Fig. 4. TGA and DTA curves of ASR with 15 wt.% NiO/Al_2O_3 catalyst (ASR/catalyst wt. ratio = 50 and S/O/C = 1.4/1.2/1.0) from 400 to 973 K at a heating rates of (a) 15, (b) 10, and (c) 5 K min^{-1} in a mixing flow of 15.3 vol.% O_2 and steam (100 mL min^{-1}).

provides information of electronic configuration, stereochemistry and the oxidation states of nickel species [21–28]. In Fig. 2, the pre-edge XANES spectrum of NiO/Al_2O_3 catalysts exhibits a very weak absorbance feature for the 1s-to-3d transition, which is forbidden by the selection rule in the case of perfect octahedral symmetry [51]. The intensity of the 1s-to-$4p_{xy}$ transition was proportional to the population of Ni(II) or Ni(0) on Al_2O_3 in the ASR catalytic gasification process [52,53]. A shoulder at 8330–8333 eV and an intense feature at 8340–8350 eV were attributed to the 1s-to-$4p_{xy}$ transition, that indicated the existence of Ni(II) species on Al_2O_3 in the ASR catalytic gasification process [52–55]. However, the upshift of the edge energy and a very weak absorption feature for 1s-to-3d forbidden transition near the pre-edge was also confirmed through the observation. The XANES spectra worked particularly well in distinguishing of Ni(0) and Ni(II) species on Al_2O_3 support. In the ASR catalytic gasification process, we found that most of the Ni(II) was reduced to Ni(0).

Basic understanding at this scale is essential for further understanding the catalytic behaviors of Ni or NiO on Al_2O_3 in the ASR catalytic gasification process. Generally, Ni K-edge EXAFS spectroscopy can provide the information on the Ni atomic arrangement of catalysts in terms of bond distance, number and kind of near

Table 3
Kinetic parameters of a lab-scale catalytic gasification system of ASR.

Carrier gas (vol.% O_2)	E_a (kcal mol^{-1})	ln A_p (min^{-1})	n	m
10.5	19.73	26.38	1.24	0.53
15.3	17.31	24.66	1.42	0.71
21.0	11.22	21.79	1.58	0.92

neighbors or thermal and static disorders [54]. The features of the XANES spectrum of NiO are significantly different from those of Ni foil; i.e., sharp absorption is observed at ca. 8350 eV for that of NiO [55]. An over 99% reliability of the Fourier-transformed EXAFS data fitting for NiO or Ni species on Al_2O_3 was obtained (Fig. 3). Standard deviation calculated from the averaged spectra was also determined. In all EXAFS data analyzed, the Debye–Waller factors ($\Delta\sigma^2$) were less than 0.02 $Å^2$. As shown in Fig. 3(a) and (b), central Ni atoms have a Ni–O and a Ni–Ni with bond distances of 2.04 ± 0.05 and 2.48 ± 0.05 Å, respectively on Al_2O_3 support. According with the Takenaka et al. [56] the peaks around at 2.04 ± 0.05 Å ascribed to the presence of Ni–O and is not easily reduced by hydrogen. In addition, the intensities of the peaks around 2.48 ± 0.05 Å were weak in the Fourier transforms of the EXAFS of used NiO/Al_2O_3. These peaks would be mainly due to Ni–Ni bond structure. Therefore, it is likely that Ni species in used NiO/Al_2O_3 were highly dispersed. Furthermore, ASR oxidation is occurred on the NiO/Al_2O_3 surface to produce metallic Ni species, could be the formation of tar/char in the gasification process. Since the complete ASR combustion might be reduced into the tar/char content with the production of hydrogen rich syngas, higher oxygen affinity of metallic nickel could be postulated as the formation of $NiAl_2O_4$. Therefore, EXAFS data revealed that the reduction in tar/char content prior to Ni catalysts was identified as a possible way to maintain the activity of the catalysts. Moreover, deactivation of the catalysts might occur as a result of carbon fouling and also of thermal sintering.

3.2. Proximate, ultimate, and kinetics analyses of ASR

Table 2 indicates the results of elemental analyses of ASR where combustible content such as volatile or fixed carbon constitutes are the main component of a typical ASR mixture. Low moisture and high ash content in light or heavy ASR are also notably observed. Moreover, carbon is the main component and few chlorine and sulfur are present in both kinds of ASR mixtures. Typical TGA curves for ASR catalytic gasification are shown in Fig. 4. A one-stage process for thermal degradation of ASR is observed and a pseudo-first

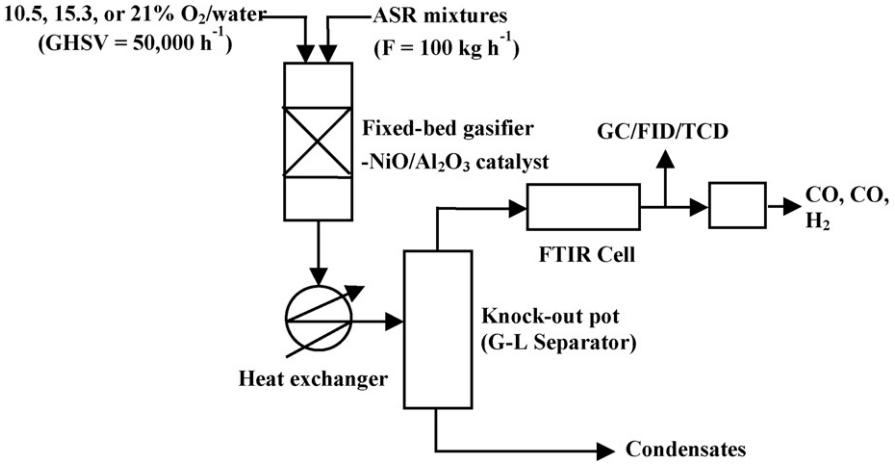

Fig. 5. A schematic flow diagram of a lab-scale catalytic gasification system for ASR on 15 wt.% NiO/Al_2O_3 catalyst at 760–900 K and 1 atm.

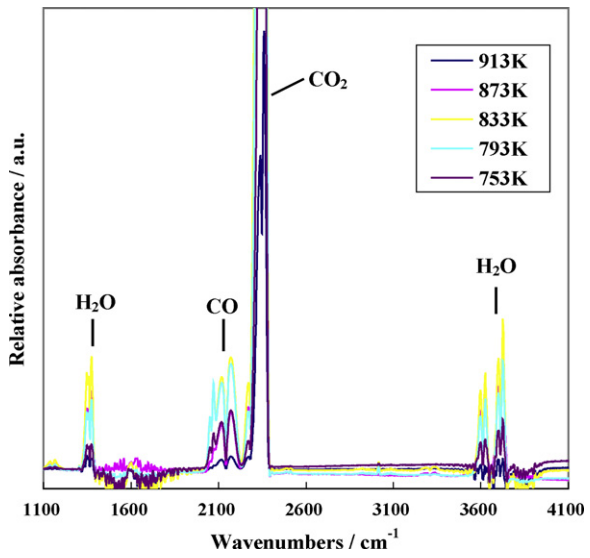

Fig. 6. FTIR spectra of syngas produced from the ASR catalytic gasification with 15 wt.% NiO/Al_2O_3 catalyst at T = 753–913 K and 1 atm.

order ASR catalytic gasification reaction has therefore approached. Since the lower mass transfer resistance, the TGA curves of more complete and effective ASR gasification reaction with higher heating rates may shift to lower gasification temperatures. The derived kinetic parameters of ASR gasification from the thermogravimetry experiments are summarized in Table 3. The catalytic gasification of ASR can be satisfactorily described by the corresponding rate equation.

$$\frac{dX}{dt} = (1.16 \pm 0.40 \times 10^{10}) \exp\left(\frac{-15.5 \pm 4.5}{1.987 \times 10^{-3} T}\right) \times (1-X)^{1.4\pm0.2}[O_2]^{0.7\pm0.2}$$

The conversion and residence time are the main engineering design data used in sizing the reactor as well as optimizing operation conditions. The gasification temperature, on the other hands, is the key factor for determining the desired product distribution. As shown in Fig. 5, it indicates that the distribution of activation energy (E_a) calculated from catalytic gasification kinetics for ASR was between 11–20 kcal mol^{-1}. The catalytic gasification of ASR represents the pseudo-first order reaction and the oxygen component is in the order of 0.7 ± 0.2. Moreover, the relatively lower activation energy of ASR catalytic gasification indicated that this reaction may be easily achieved and the potential of hydrogen generation from ASR gasification was observed. Only one distinct weight loss stage of the ASR gasification is found. In the stage of temperatures around 780 K, high concentrations of gaseous CO_2 and CO are exhausted and also observed by on-line FTIR spectroscopy shown in Fig. 6 that may be caused mainly by thermal degradation of ASR in the catalytic gasification processes. In addition, according to Fig. 4 in an ASR catalytic gasification process, the reaction rate of the highly exothermic and rapid water-shift reaction are decreased with increasing shift temperatures from 753 to 913 K, indicating that an increase in the reaction temperature favored the formation of H_2 and decomposition of the CO. The higher concentrations of CO_2 and H_2O are also observed in higher reaction or drying temperatures.

In this study, five typical infrared spectra for the syngas generated from the ASR catalytic gasification at T = 753–913 K and 1 atm were shown in Fig. 6. As expected, the stretching band of CO, CO_2 and H_2O gases are observed at 2005–2250, 2250–2370, and 3700–3950 (or 1500–1800) cm^{-1}, respectively, obviously indicating that the catalytic gasification reactions have occurred. In addition, in the presence of the catalyst, an ASR may have higher gasification on CO production then without catalyst. Therefore the intensity of the CO formation at 2005–2250 cm^{-1} is significantly lower, implying an incomplete reaction involved in the complicated noncatalytic gasification of ASR with strong bonding of aliphatics or paraffins. This result may be caused mainly by the high-molecular-weight components in ASR, which were not completely destroyed at a lower gasification temperature of 900 K without catalyst [57–59]. Since the composition of ASR is very complicated, the catalytic gasification of ASR may produce some additional by-products. Among them, sulfur in the ASR was primarily react with Ni catalyst to form NiS and then converted into H_2S, which was easily removed from the syngas by conventional cleanup methods. Since the Ni–O bonding is weaker than Ni–S bonding, hydrogen sulfide is then oxidized with water to sulfur dioxide with formation of hydrogen ($H_2S + 2H_2O \leftrightharpoons SO_2 + 3H_2$) [60,61]. Nitrogen was converted into N_2, with minor traces or no detected of NH_3, which might readily be dissolved in the process water and neutralized with the acidic feed components such as chlorides. Finally, little NO_x or SO_x may be formed due to the chemically reducing atmosphere in the ASR catalytic gasifier [38].

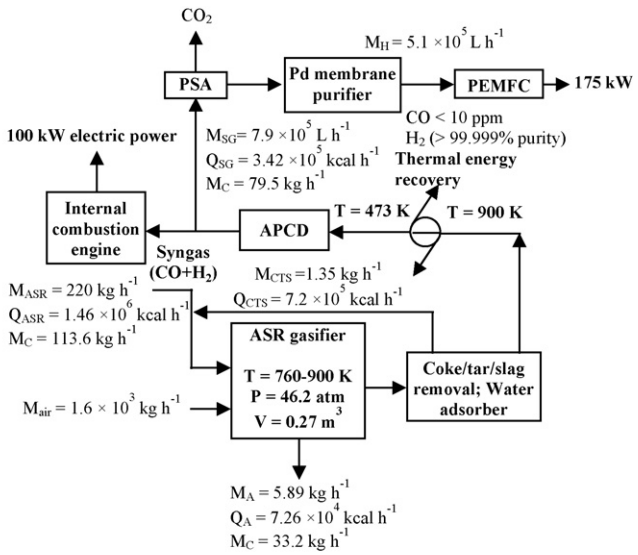

Design basis: 100 kW h^{-1} of electric power generated from ASR catalytic gasification.

Note:
1. Eight hours operation per day with preheating the catalytic gasifier by natural gas;
2. Assuming tar or slag was produced from 0.5% unconversion carbon of ASR catalytic gasification;
3. Assuming O/C mole ratio = 1.10-1.30;
4. A, C, ASR, SG, H, and CTS denote the mass of ashes, carbon, automotive shredder residues, syngas, hydrogen, and coke/tar/slag, respectively.
5. PSA and APCD denote "pressure swing adsorption and air pollution control device, respectively.
6. The performance results of 100 cm^2 four cells with 169 cm^2 bipolar-plane area at gas humidified temperature 348 K and cell temperature at 343 K. The specification conditions are as following: MEA type = Gore/PRIMEA series 5510 MEAs; catalyst loading = 0.8 g cm^{-2}; flow-field type = 16 serpentines; Fuel flow rate H_2/Air = 1.2/2.5; cooling type = water cooling; catalyst reaction area 100 cm^2 at operating condition of 0.5 V (basis = 200 W per unit).

Fig. 7. Material and energy balances of a pilot-scale ASR catalytic gasification process with hydrogen generation in an integrated fuel processor.

3.3. Basic design of an ASR catalytic gasification process

In this work, experimental data obtained from a lab-scale ASR catalytic gasification system can be used as the basis for the scale-up of this technology. In that follows, some simulation calculations and parameter evaluations were given for this system with the

Table 4
Design basis of a 10-TPD catalytic gasification system of ASR for an integrated fuel processor.

Design philosophy	
Downdraft-type catalytic gasification system	
Continuous operation	
Individual units to be as stand-alone as possible	
Moderate-to-high level of automation	
Major design parameters	
Feeds	
Well-mixed ASR without pretreatment	
Air and/or steam	
Operational conditions	
Feed rate	10-TPD
Volume of gasifier	0.27 m^3
Heat loss	5.35×10^3 kcal h^{-1}
Unconversion carbon	0.5%
O/C	1.1–1.3 atom/atom
T, *P*	900 K, 46.2 atm
Desired power output	100 kW
Ultimate product fate	
Ash	
Reclaimed in carbon steel manufacturing	
Syngas	
Fuel gas ($CO + H_2$ = 87%, dry basis)	
Generation of electric power	
CO	
Shift to hydrogen	
H_2	
Recycling (supply for an integrated fuel processor or others)	
Composition of syn gas (unit: mol%)	
CO	32.8
CO_2	10.8
H_2	54.2
N_2	1.6
CH_4	0.5
HCl	<0.01
H_2S	<0.01
COS	<0.01
Cold gas efficiency	76–85%
Heat recovery	3.42×10^5 kcal h^{-1}

reaction or equilibrium equations using EXCEL software. The principal operational units in the united gasification of simulated ASR include a gasifier section (including a CO shift section), H_2 purification section (pressure swing adsorption (PSA) and Pd membrane purifier), and a final PEMFC are represented in Fig. 7 [62,63]. The particulate free and saturated syngas are obtained from the simulated ASR streams gasification unit. This unit employed one or two fixed catalytic beds to convert CO and steam into CO_2 and H_2. The water gas shift reaction can be simply expressed by the following equation: $CO + H_2O$ (CO shift conversion) $\rightarrow CO_2 + H_2$ ($\Delta H = -8.093$ kcal mol^{-1} at 900 K) [57–59]. Since the reaction was highly exothermic, a conventional heat-recovery exchanger could be used to generate medium-pressure steam for export or captive consumption. The effluent gas from the CO shift unit was then fed to a PSA unit for H_2 purification with Pd membranes. Adsorbent beds at high pressure removed the impurities and a high-purity (>99.99%) H_2 stream was effectively produced shown in Fig. 7 [62,63]. The adsorbed impurities were then concentrated and removed at low pressure in the form of a reject-gas stream. Depending on the feedback characteristics, the reject gas can be partially recycled to the process, or used in the refinery or petrochemical industries. As shown in Fig. 7, the material and energy balances of an ASR catalytic gasification process may provide the essential information about the operational condition in the system and determine if further developments would be warranted. The process consists of an ASR feed system, a downdraft-type gasifier, an ash discharge system, a coke/tar/slag or water adsorber, an internal combustion engine for power generation, CO/H_2 separator, hydrogen purifier, and an integrated fuel processor. Simulated data indicate that approximately 220 kg h^{-1} of ASR would be catalytically gasified at 760–900 K and 46.2 atm with the reactor volume 0.27 m^3 for the generation of 100 kW electric power. The global material balance for this catalytic gasification process was >96%. An illustration of the process design concept for the treatment of the simulated ASR with catalytic gasification system from Fig. 7 is shown in Table 4. In the simulated pilot-scale continuous operation of downdraft-type ASR catalytic gasification system included with individual units to be as stand-alone as possible in moderate-to-high level of automation was carried out with temperatures were much higher than 700 K and the main products were CO and H_2. In addition, the pressure of an ASR catalytic gasifier was usually based on the pressure required for the delivery of the ultimate product (CO or H_2) to its end use (for instance, an integrated fuel processor or the refinery hydrogen header pressure) and purification is carried out through a PSA to separate CO_2. Generally, operating pressures in the commercial biowastes or coal noncatalytic gasification processes are ranged from 50 to 80 atm [40–45]. It is noteworthy that a commercial catalytic gasifier often operates at mid-term temperatures or pressures and a well-mixed gaseous environment in which the partial oxidation reactions take place. ASR catalytic gasification reaction ($ASR + O_2 + H_2O \rightarrow CO + H_2$) and the CO water-shift reaction ($CO + H_2O \rightarrow CO_2 + H_2$) were also influenced by both the O/C ratio and shift temperature of the catalytic gasifier. Specific oxygen consumption (SOC) and cold gas efficiency (CGE) values of an ASR catalytic gasification process are increased and decreased, respectively. Increase of O/C ratio are also enhanced the ASR catalytic gasification. Approximately 3.42×10^5 kcal h^{-1} of thermal energy may be recovered from the ASR catalytic gasification process at the temperatures from 700 to 1100 K, indicating that an increase in the reaction temperature favored the formation of H_2 and decomposition of the CO [26–28,30]. The CGE may reach 76–85% when the catalytic gasifier process is operated at the O/C ratios between 1.13 and 1.30. It should be noted that theses results are also consistent with the FTIR spectra shown in Fig. 6.

4. Conclusions

The feasibility for an ASR catalytic gasification was investigated. Based on the catalytic gasification experimental data obtained from the lab-scale downdraft-type reaction system, the primary engineering design for a pilot plant of the ASR catalytic gasification process was also accomplished. It appears that approximately 220 kg h^{-1} of ASR would be gasified to generate 100 kW electric power. A 10-TPD pilot plant of ASR treatment facility is currently under construction in Fuel Cell Center of Yuan Ze University, Taiwan to prove technical and economic viability of the ASR catalytic gasification process concept. In the ASR catalytic gasification process, most of the Ni(II) reduced to Ni(0) was found by XANES spectra. The EXAFS data also showed that the central Ni atoms had a Ni–O and a Ni–Ni with bond distances of 2.04 ± 0.05 and 2.48 ± 0.05 Å, respectively on Al_2O_3 support. Thus, the peaks around at 2.04 ± 0.05 Å ascribed to the presence of Ni–O bonding was not reduced easily by the reduction with hydrogen. In addition, the intensities of the peaks around 2.48 ± 0.05 Å were weak in the Fourier transforms of the EXAFS of Ni/Al_2O_3. These peaks would be due to Ni–Ni bonding mainly. Therefore, it is likely that Ni species in Ni/Al_2O_3 were highly dispersed. Thus, a complete gasification of ASR occurred to form Ni on the catalyst surface and start to generate the production of hydrogen. The material and energy balances of the 10-TPD ASR gasification system pointed out that >87% (dry basis) of H_2 and CO were generated at 900 K and 46.2 atm, and approximately 3.42×10^5 kcal h^{-1} of thermal energy were recovered. In addition, the catalytic gasification of ASR to syngas, production of high-purity hydrogen, and final processing to make it suitable for the integrated fuel cell power generation system.

Acknowledgement

The financial supports of National Science Council (contract no.: NSC-94-2211-E-155-001) of Taiwan, R.O.C. are gratefully acknowledged.

References

[1] ROC EPA, A Planning Report for the Recycling Strategies of Automotive Shredder Residues, EPA, ROC, EPA-95-06-411, 2006.
[2] O. Gonzalez-Fernandez, M. Hidalgo, E. Margui, M.L. Carvalho, I. Queralt, Environ. Pollut. 153 (2008) 476–482.
[3] M.K. Harder, O.T. Forton, J. Anal. Appl. Pyrolysis 79 (2007) 387–394.
[4] M. Nourreddine, J. Hazard. Mater. A139 (2007) 481–490.
[5] M.H. Lopes, M. Freire, M. Galhetas, I. Gulyurtlu, I. Cabrita, Waste Manag. 29 (2009) 1760–1765.
[6] J.G. Seo, M.H. Youn, K.M. Cho, S. Park, I.K. Song, J. Power Sources 173 (2007) 943–949.
[7] T. Davidian, N. Guilhaume, E. Iojoiu, H. Provendier, C. Mirodatos, Appl. Catal. B: Environ. 73 (2007) 116–127.
[8] K.S. Lin, C.K. Lee, J. Pract. Period. Hazard. Toxic Radioact. Waste Manag. 10 (2006) 150–155.
[9] J.L. Pinilla, I. Suelves, R. Utrilla, M.E. Gálvez, M.J. Lázaro, R. Moliner, J. Power Sources 169 (2007) 103–109.
[10] F. Jahnke, TAPPI J. 82 (1999) 49–53.
[11] M. Horii, S. Iida, JSAE Rev. 22 (2001) 63–68.
[12] M. Kondoh, M. Hamai, M. Yamaguchi, S. Mori, Technical Notes/JSAE Rev. 22 (2001) 221–236.
[13] T. Kan, J. Xiong, X. Li, T. Ye, L. Yaun, Y. Torimoto, M. Yamamoto, Q. Li, Int. J. Hydrogen Energy 35 (2010) 518–532.
[14] A. Sharma, H. Nakagawa, K. Miura, Fuel 85 (2006) 179–184.
[15] L.I. Darvell, K. Heiskanen, J.M. Jones, A.B. Ross, P. Simell, A. Williams, Catal. Today 81 (2003) 681–692.
[16] M.H. Youn, J.G. Seo, P. Kim, J.J. Kim, H.I. Lee, I.K. Song, J. Power Sources 162 (2006) 1270–1274.
[17] R. Toonssen, N. Woudstra, A.H.M. Verkooijen, J. Power Sources 194 (2009) 456–1466.
[18] M. Benito, S. García, P.F. Aparicio, L.G. Serrano, L. Daza, J. Power Sources 169 (2007) 177–183.
[19] K. Sato, K. Fujimoto, Catal. Commun. 8 (2007) 1697–1701.
[20] T. Kimura, T. Miyazawa, J. Nishikawa, S. Kado, K. Okumura, T. Miyao, S. Naito, K. Kunimori, K. Tomishige, Appl. Catal. B: Environ. 68 (2006) 160–170.
[21] A. Sharma, I. Saito, H. Nakagawa, K. Miura, Fuel 86 (2007) 915–920.
[22] B. Li, K. Maruyama, M. Nurunnabi, K. Kunimori, K. Tomishige, Ind. Eng. Chem. Res. 44 (2005) 485–494.
[23] M. Inaba, K. Murata, M. Saito, I. Takahara, Energy Fuels 20 (2006) 432–438.
[24] L. Garcia, A. Benedicto, E. Romeo, M.L. Salvador, J. Arauzo, R. Bilbao, Energy Fuels 16 (2002) 1222–1230.
[25] C. Courson, L. Udron, D. Świerczyński, C. Petit, A. Kiennemann, Catal. Today 76 (2002) 75–86.
[26] L. Wang, K. Murata, Y. Matsumura, M. Inaba, Energy Fuels 20 (2006) 1377–1381.
[27] K. Matsuoka, T. Shinbori, K. Kuramoto, T. Nanba, A. Morita, H. Hatano, Y. Suzuki, Energy Fuels 20 (2006) 1315–1320.
[28] L. Huang, J. Xie, W. Chu, R. Chen, D. Chu, A.T. Hsu, Catal. Commun. 10 (2009) 502–508.
[29] K. Tomishige, T. Kimura, J. Nishikawa, T. Miyazawa, K. Kunimori, Catal. Commun. 8 (2007) 1074–1079.
[30] T. Wang, J. Chang, X. Cui, Q. Zhang, Y. Fu, Fuel Process. Technol. 87 (2006) 421–428.
[31] S. Campanari, G. Manzolini, F.G.D.L. Iglesia, J. Power Sources 186 (2009) 464–477.
[32] R. Martínez, E. Romero, L. García, R. Bilbao, Fuel Process. Technol. 85 (2003) 201–214.
[33] A. Sharma, H. Nakagawa, K. Miura, Fuel 85 (2006) 2396–2401.
[34] S.C. Tsang, J.B. Claridge, M.L.H. Green, Catal. Today 23 (1995) 3–15.
[35] P.V. Aravind, T. Woudstra, N. Woudstra, H. Spliethoff, J. Power Sources 190 (2009) 461–475.
[36] C. Cellier, B. Blangy, C. Mateos-Pedrero, P. Ruiz, Catal. Today 112 (2006) 112–116.
[37] F. Patcas, F.C. Patcas, Catal. Today 117 (2006) 253–258.
[38] Z.A. El-Rub, E.A. Bramer, G. Brem, Ind. Eng. Chem. Res. 43 (2004) 6911–6919.
[39] P. Forzatti, L. Lietti, Catal. Today 52 (1999) 165–181.
[40] K.S. Lin, H.P. Wang, C.J. Lin, C.I. Juch, Fuel Process. Technol. 55 (1998) 185–192.
[41] A.S. Damle, J. Power Sources 186 (2009) 167–177.
[42] P. Ji, W. Feng, H.J.V. Kooi, J.D.S. Arons, Ind. Eng. Chem. Res. 43 (2004) 2005–2016.
[43] M.P. Aznar, M.A. Caballero, J. Corella, G. Molina, J.M. Toledo, Energy Fuels 20 (2006) 1305–1309.
[44] S.M. Swami, M.A. Abraham, Energy Fuels 20 (2006) 2616–2622.
[45] S.M. de Lima, R.C. Colman, G. Jacobs, B.H. Davis, K.R. Souza, A.F.F. de Lima, L.G. Appel, F.B. Noronha, Catal. Today 146 (2009) 110–123.
[46] Z.S. Petrović, Z.Z. Zavargo, J. Appl. Polym. Sci. 32 (1986) 4353–4367.
[47] H.L. Friedman, J. Polym. Sci. Part C 6 (1964) 183–195.
[48] F.W. Lytle, J. Synchrotron Radiat. 6 (1999) 123–134.
[49] A.I. Nesvizhskii, J.J. Rehr, J. Synchrotron Radiat. 6 (1999) 315–316.
[50] T. Resslert, J. Synchrotron Radiat. 5 (1998) 118–122.
[51] M.-J. Paek, T.W. Kim, S.-J. Hwang, J. Phys. Chem. Solids 69 (2008) 1444–1446.
[52] F. Farges, G.E. Brown Jr., P.E. Petit, M. Munoz, Geochim. Coscochim. Acta 65 (2001) 1665–1678.
[53] L. Galoisy, L. Cormier, G. Galas, V. Briois, J. Non-Cryst. Solids 293–295 (2001) 105–111.
[54] R.F.D. Souza, L.C. Simon, M.D.C.M. Alves, J. Catal. 214 (2003) 165–168.
[55] S. Takenaka, E. Kato, Y. Tomikubo, K. Otsuka, J. Catal. 219 (2003) 176–185.
[56] S. Takenaka, H. Ogihara, I. Yamanaka, K. Otsuka, Appl. Catal. A: Gen. 217 (2001) 101–110.
[57] J.A.C. Dias, J.M. Assaf, J. Power Sources 137 (2004) 264–268.
[58] G. Egloff, E.F. Nelson, J.C. Morrell, Ind. Eng. Chem. 29 (1937) 555–559.
[59] D. Gourgouillon, L. Schrive, S. Sarrade, G.M. Rios, Environ. Sci. Technol. 34 (2000) 3469–3473.
[60] J. Srinakruang, K. Sato, T. Vitidsant, K. Fujimoto, Fuel 85 (2006) 2419–2426.
[61] C. Lombard, S.L. Doze, E. Marencak, P.M. Marquaire, D.L. Noc, G. Bertrand, F. Lapicque, Int. J. Hydrogen Energy 31 (2006) 437–440.
[62] G. Chiappetta, G. Clarizia, E. Drioli, Chem. Eng. J. 124 (2006) 29–40.
[63] R. Chaney, L.V. Bibber, Beluga Coal Gasification Feasibility Study, DOE/NETL-2006/1248, Phase I, Final Report for Subtask 41817.333.01.01, July 2006.